

# Laser Treatment of Ag@ZnO Nanorods as Long-Life-Span SERS Surfaces

Manuel Macias-Montero,<sup>\*,†</sup> Ramón J. Peláez,<sup>‡</sup> Víctor J. Rico,<sup>†</sup> Zineb Saghi,<sup>§</sup> Paul Midgley,<sup>§</sup> Carmen N. Afonso,<sup>‡</sup> Agustín R. González-Elipe,<sup>†</sup> and Ana Borrás<sup>†</sup>

<sup>†</sup>Nanotechnology on Surfaces Laboratory, Materials Science Institute of Seville (ICMS), CSIC-University of Seville, C/AmericoVespucio 49, 41092 Seville, Spain

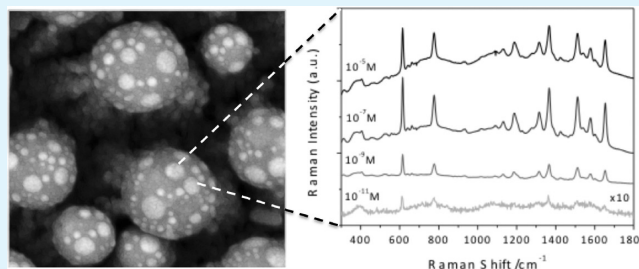
<sup>‡</sup>Laser Processing Group, Instituto de Optica, CSIC, Serrano 121, 28006 Madrid, Spain

<sup>§</sup>Department of Materials Science and Metallurgy, University of Cambridge, 27 Charles Babbage Road, Cambridge CB3 0FS, United Kingdom

## S Supporting Information

**ABSTRACT:** UV nanosecond laser pulses have been used to produce a unique surface nanostructuring of Ag@ZnO supported nanorods (NRs). The NRs were fabricated by plasma enhanced chemical vapor deposition (PECVD) at low temperature applying a silver layer as promoter. The irradiation of these structures with single nanosecond pulses of an ArF laser produces the melting and reshaping of the end of the NRs that aggregate in the form of bundles terminated by melted ZnO spherical particles. Well-defined silver nanoparticles (NPs), formed by phase separation at the surface of these melted ZnO particles, give rise to a broad plasmonic response consistent with their anisotropic shape. Surface enhanced Raman scattering (SERS) in the as-prepared Ag@ZnO NRs arrays was proved by using a Rhodamine 6G (Rh6G) chromophore as standard analyte. The surface modifications induced by laser treatment improve the stability of this system as SERS substrate while preserving its activity.

**KEYWORDS:** Ag@ZnO nanorods, low-temperature plasma growth, laser treatment, long-life-span SERS



## 1. INTRODUCTION

Metal nanoparticles are known to generate large electromagnetic field enhancements via surface plasmon resonance (SPR) effects that have a high impact in different optical spectroscopies including linear absorption or Raman. SPR features are known to depend on the size, shape, and association of the NPs as well as on the type of metal and the dielectric environment around them.<sup>1–4</sup> This dependence has been exploited for the fabrication of dichroic filters,<sup>5,6</sup> polarized light nanostructures,<sup>7,8</sup> materials with second-order nonlinearities,<sup>9</sup> several sensing applications<sup>10</sup> or surface-enhanced resonance spectroscopy (SERS) sensors. In particular, because of its high sensitivity, rapid response, and fingerprint management, SERS has developed rapidly for its tremendous potentials in chemical and biological sensing.<sup>11,12</sup> In this spectroscopy, the Raman bands of organic molecules experience an enhancement by several orders of magnitude when they are adsorbed on silver nanoparticles and therefore affected by the evanescent field of the SPR field.<sup>13</sup>

The increase of the evanescent field, deemed responsible for the SERS effect, is higher at neck interconnections between associated NPs<sup>14</sup> or in metal/semiconductor heterostructures enabling specific metal–semiconductor interface interactions.<sup>15,16</sup> In fact, some semiconductors such as ZnO can also

generate weak SERS activity with prominent enhancement factors up to  $1 \times 10^3$ .<sup>17</sup> Similarly, Ag or Au NPs in contact or deposited on semiconductor nanorods or nanowires of Si, Ge or ZnO, have led to significant enhancements in Raman scattering.<sup>18,19</sup> These evidence have prompted the study of composites or heterostructures formed by semiconductors and noble metals to promote higher SERS effects due to the contributions of both an electromagnetic enhancement (excited by the localized SPR of noble metals) and a semiconductor supporting electromagnetic enhancement (caused by the charge transfer between the noble metal and the adjacent semiconductor).<sup>20–23</sup>

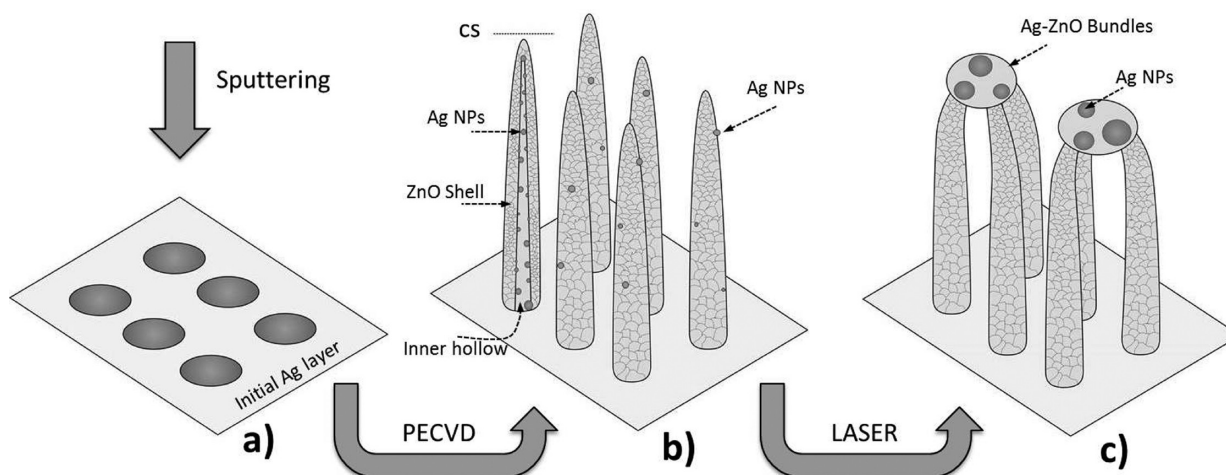
Enhancement of the sensing response is also observed in hollow one-dimensional nanostructures with a high surface to volume ratio.<sup>24–29</sup> In previous works, we have reported a route to produce supported hollow NRs of ZnO which were decorated with silver nanoparticles.<sup>30,31</sup> The fabrication method consisted of a plasma-enhanced chemical vapor deposition (PECVD) procedure.<sup>30,31</sup> This system, with a high surface area and a high concentration of silver NPs, has an ideal

**Received:** September 29, 2014

**Accepted:** January 9, 2015

**Published:** January 9, 2015

**Scheme 1. Illustration of the Synthesis Process of Ag@ZnO Complex Nanostructures: (a) Initial Ag Layer Deposited by DC-Sputtering; (b) Ag@ZnO NRs Grown by PECVD, Highlighting the Components on a Single NR Cross-Section (CS); and (c) Laser-Treated Ag-ZnO Nanostructures, Showing a Characteristic Association of Their Upper Part and the Formation of ZnO Particles with Embedded Larger Ag NPs**



nanostructure for the development of a SERS sensor system. Another advantage of this system for SERS resides in its vacuum-based methodology that circumvents potential spectral interference caused by remaining chemical agents used during chemical wet methods.<sup>32</sup> However, a problem encountered by its use for SERS sensing is a progressive decrease in sensitivity when utilized successive times. The observed association of the supported NRs in the form of nanocarpet when dripping water on their surface<sup>33</sup> is deemed as the main responsible factor for this decrease in sensitivity.

To overcome this limitation UV nanosecond laser pulses have been applied to induce specific surface modifications contributing to keep the efficiency of the original material as a long lasting SERS substrate. Laser irradiation with UV nanosecond laser pulses has been used to improve the structural or optical properties of ZnO NRs, the latter evidenced by an overall enhancement of the UV photoluminescence (PL).<sup>34–36</sup> This treatment has been also proved to be a useful tool for increasing the on-current NRs field effect transistor.<sup>37</sup> In all these experiments, there were microstructural changes affecting the end of the NRs that can be related to surface melting processes induced by laser. The characteristics of the obtained nanostructures depended on the utilized laser fluence: coarsening is generally observed for low fluences, while formation of spherical NPs,<sup>37,38</sup> clustering of adjacent NRs,<sup>35,37</sup> or even offal NRs leading to an irregular coating on top of the NRs<sup>36</sup> have been found for high fluences.

In the present work, we show that NRs tip melting and association and the formation of embedded anisotropic Ag nanoparticles are the main structural changes induced by laser. These changes prevent the nanocarpet association of NRs by water dripping<sup>33</sup> and contribute to the stabilization of the Ag@ZnO NRs structure for its long-lasting use as SERS sensing substrates. Besides disclosing the nature of the laser-induced microstructural changes, it has been also found that reshaped Ag NPs are responsible for a polarization sensitive plasmonic response of these laser transformed materials.

## 2. EXPERIMENTAL METHODS

The fabrication process steps of supported Ag@ZnO nanostructures are shown in Scheme 1. First, silver NPs are deposited by DC-

sputtering at room temperature onto different substrates. Additional information about this procedure can be found elsewhere.<sup>39,40</sup> These NPs act as metal seeds for the growth of Ag@ZnO NRs by PECVD at low temperatures. Then, nanosecond pulses from a UV laser are used to transform the surface of the NRs. This transformation implies their tip partial melting with the subsequent formation of ZnO particles that act as NR aggregation templates. In the course of this process, newly formed Ag NPs also become incorporated into these oxide particles.

**2.1. Fabrication of the Supported Ag@ZnO-NRs.** Polycrystalline Ag@ZnO core@shell NRs were fabricated by PECVD of diethyl zinc precursor on silver sputtered substrates (Si(100), fused silica and glass). The silver, acting as seed layer for the posterior deposition of ZnO by PECVD, was deposited by sputtering from a metal wire under a pressure of 1 Torr of Ar and an applied voltage of 400 V for 2 h. The plasma reactor consisted of a microwave electron cyclotron resonance setup working in a downstream configuration. The deposition of ZnO was carried out at 135 °C in the plasma reactor supplied with oxygen ( $5 \times 10^{-3}$  Torr) and excited with a microwave power of 400W. Diethylzinc (purchased from Sigma), used as precursor of zinc, was dosed directly in the deposition chamber at a rate of 1.2 sccm for 1 h. A set of 20 identical samples were prepared following the described procedure. These conditions produce the growth of composite nanostructures consisting of hollow ZnO NRs decorated internally by silver nanoparticles. A thorough description of the obtained materials and additional experimental details can be found elsewhere.<sup>30,31</sup>

**2.2. Laser Treatment of Supported Ag@ZnO NRs.** The Ag@ZnO NRs samples as taken from the PECVD reactor were exposed in air to single and multiple 20 ns pulses from an excimer laser operating at 193 nm. A beam homogenizer was used to enable constant beam intensity exposures (within 5%) over  $4 \times 4$  mm<sup>2</sup> square regions. For the experiments, we have used four irradiation fluences in the range 44–130 mJ cm<sup>-2</sup>.

**2.3. Characterization.** NRs arrays deposited on silicon wafers were characterized by scanning electron microscopy (SEM). The analysis of selected irradiated areas of samples deposited on fused silica substrates yielded identical results than on silicon wafers. A field emission apparatus, S4800 from Hitachi, was used for these studies. An in-depth characterization of as prepared Ag@ZnO NRs before laser irradiation was carried out using high-angle annular dark field scanning transmission electron microscopy (HAADF-STEM). The NRs were removed from the substrates and then placed in a holey carbon grid (from Agar). HAADF-STEM electron tomography was performed on a FEI Tecnai F20 field emission gun transmission electron microscope operated at 200 kV.

The extinction spectra expressed as  $\ln(1/T)$  were determined from the transmittance spectra ( $T$ ) recorded for the samples deposited on fused silica normalized to the spectrum of the bare substrate. The recording system consisted of a Mercury-Xe lamp, a polarizer and a visible fiber optics spectrometer. Spectra were recorded in the range of 400–750 nm at both  $0^\circ$  and  $45^\circ$  angle of incidence with respect to the normal to the substrate and for light polarized parallel (p-polarization) and perpendicular (s-polarization) to the incidence plane. Since for  $0^\circ$  incidence angles the spectra were not affected by the polarization of light, we will refer to the corresponding experiments by just mentioning the angle of incidence. For  $45^\circ$  incidence experiments, the type of polarized light will be also mentioned.

Raman spectra were collected in a LabRAM HR High Resolution 800 Confocal Raman Microscope. For the measurements a green laser (He–Ne 532.14 nm), 600 line/mm, 100x objective, 20 mW and 100  $\mu$  pinhole, was used. Rh6G was used as SERS probe. Different amounts of this dye molecule were dissolved in ethanol to get different solutions with concentrations ranging from  $1 \times 10^{-11}$  to  $1 \times 10^{-5}$  M. Droplets of 2  $\mu$ L were dropped on the substrate and naturally dried in air before SERS characterization.

### 3. RESULTS

**3.1. Laser Treatment of Ag@ZnO Nanorods.** Images a and b in Figure 1 shows a series of SEM images of the as-prepared samples with the supported Ag@ZnO NRs deposited on a silicon substrate. These NRs are vertically aligned and have a length of 900 nm with a typical diameter of 60 nm and a surface density of 70 NRs/ $\mu\text{m}^2$ . As reported previously and presented here in Figure 1c,<sup>30,31</sup> small silver NPs (diameter in the range 3–15 nm) are mainly distributed in an inner hollow

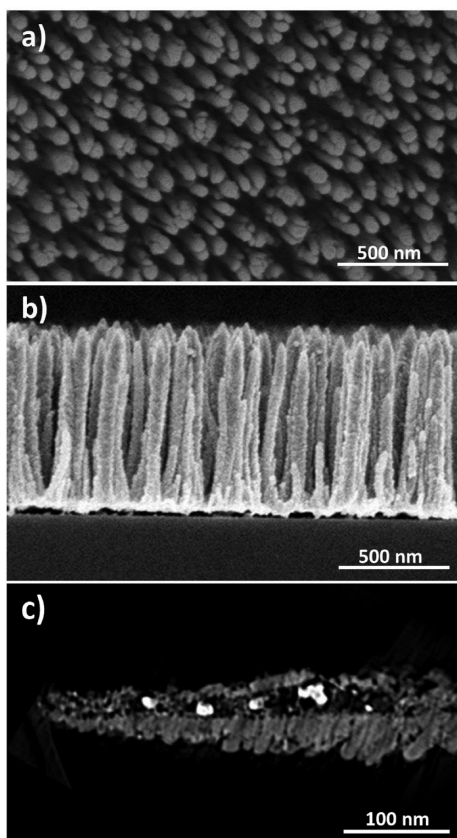


**Figure 1.** (a) Normal view and (b) cross-section SEM micrographs of vertically aligned supported Ag@ZnO NRs as grown by PECVD. (c) Vertical orthoslice of the HAADF-STEM 3D reconstruction of a single Ag@ZnO NR; bright features correspond to the Ag nanoparticles.

along the NRs. The entire NR-structure is highly porous, thus enabling the direct contact of the Ag NPs with liquids when dripping a droplet on the sample surface. The set of specimens investigated in this work had a similar morphology and spatial distribution of NRs.

An example of laser treated Ag@ZnO NRs is presented in Figure 2, where SEM images of a zone exposed to a fluence of

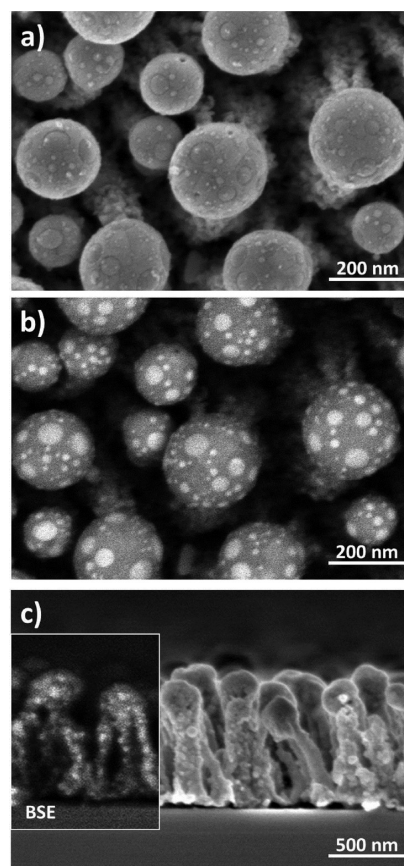


**Figure 2.** Normal view SEM micrographs of laser treated Ag@ZnONRs  $72 \text{ mJ cm}^{-2}$  using (a) secondary and (b) backscattered electrons. (c) Secondary electrons cross section image of the same preparation. The inset in c shows the corresponding backscattered electrons cross-section image of the same preparation.

$72 \text{ mJ cm}^{-2}$  are shown. The irradiation leads to the formation of almost spherical ZnO particles at the upper part of several NRs that in this way become associated in a rigid superstructure as sketched in Scheme 1c and imaged in this figure. Figure 2b shows a backscattered electron image of these rounded particles evidencing some bright areas confined to the neighborhood of the surface. These bright dots are attributed to newly formed silver NPs. It is important to stress that these structural modifications do not affect the lower part of the NRs, as evidenced by comparing the cross-section SEM micrographs of Figure 2c taken from the irradiated area and the one in Figure 1b corresponding to the as-prepared NRs. The diameter of the spherical ZnO particles and the newly formed Ag NPs are respectively in the ranges 100–200 nm and  $<50$  nm.

Figure 3 shows the dependence of the structural changes induced by laser irradiation as a function of the laser fluence. The lowest fluence, i.e.,  $44 \text{ mJ cm}^{-2}$  (Figure 3a), is close to the tip association threshold since some coarsening of the tip and incipient clustering of NRs is observed. At higher fluences ( $72$



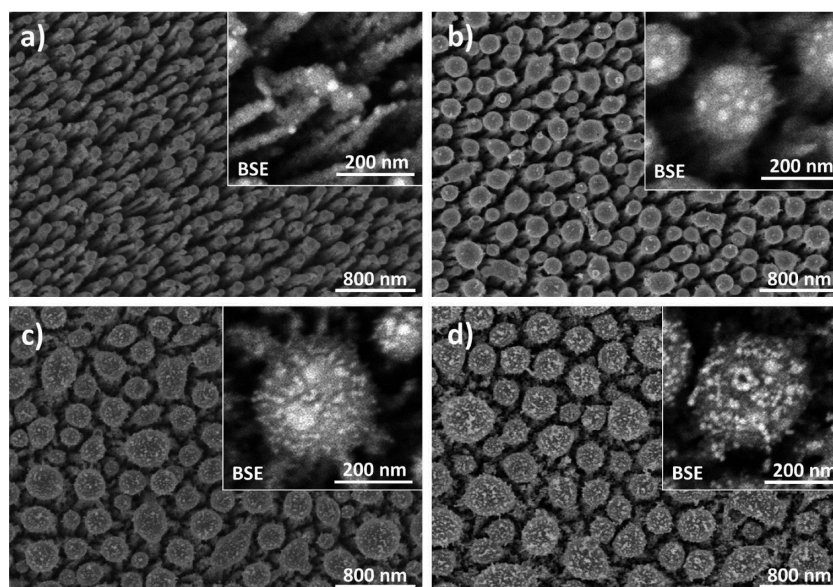


**Figure 3.** SEM micrographs of Ag@ZnO NRs laser irradiated with different power fluxes: (a)  $44 \text{ mJ cm}^{-2}$ , (b)  $72 \text{ mJ cm}^{-2}$ , (c)  $101 \text{ mJ cm}^{-2}$  and (d)  $130 \text{ mJ cm}^{-2}$ . Insets: BSE images showing the silver NPs on the bundles created after the laser treatment (sizes between 5 and 80 nm).

$\text{mJ cm}^{-2}$ , Figure 3b) several NRs become associated through a single rounded ZnO particle with a diameter increasing with the fluence. For the highest fluence ( $130 \text{ mJ cm}^{-2}$ , Figure 3d) the diameter of the ZnO particles becomes  $\sim 250 \text{ nm}$ . The Ag NPs decorating the ZnO particles also change their size and shape as the fluence increases. For low fluences (Figure 3b), Ag NPs look round and have diameters in the range 20–40 nm. At high fluences, smaller Ag NPs ( $<10 \text{ nm}$  of diameter) are observed.

To investigate the structure of the rounded ZnO particles, we performed complementary XRD and TEM measurements. Figure S1 in the Supporting Information presents XRD spectra of samples irradiated at different fluences, preserving the crystallinity in all the cases. By contrast, the XRD peaks associated with Ag depict no major alteration upon laser treatment. This would indicate that the laser treatments have produced a recrystallization of the oxide phase. Figure S2 in the Supporting Information further deepens in this aspect with TEM analysis of the ZnO particles. Selected area electron diffraction reveals the presence of crystalline ZnO and Ag. Using high-resolution TEM, it was also possible to differentiate the Ag NPs within the ZnO. In another experiment, the samples were exposed for 2, 5, and 6 times to a laser fluence of  $72 \text{ mJ cm}^{-2}$ . The SEM images, presented in Figure S3 of the Supporting Information, show that the associated structures of NRs formed after the first irradiation is stable and remains unaltered after successive laser treatments.

As prepared Ag@ZnO NRs exhibit a superhydrophobic behavior attributed to the combination of two factors: the hydrophobicity of ZnO itself and the nanostructuring of the surface.<sup>30,33</sup> Water contact angle measurements have been also carried out on laser treated Ag@ZnO NRs, where a hydrophobic behavior with a contact angle of about  $145^\circ$  was found in all cases (a picture of a water droplet on a Ag@ZnO surface can be found in Figure S4 of the Supporting Information). It is known that dripping water on the as-prepared Ag@ZnO NRs surfaces give rise to a clustering process known as nanocarpet effect.<sup>33</sup> This nanostructural modification is attributed to the compensation of capillary

forces induced by the liquid and the mechanical bounding of the NRs toward the substrate surface (a micrograph showing these surface modifications is displayed in the Figure S5 of the Supporting Information.). In contrast with this modification of the surface nanostructure by dripping water on the as-prepared NRs, SEM micrographs of wetted areas (experiments were carried out with water or ethanol) of laser modified NRs showed no major alterations of the nanostructure for samples treated with fluences higher than  $72 \text{ mJ cm}^{-2}$ . The implications of this laser mechanical stabilization of the nanostructure for sensor SERS applications will be discussed below.

**3.2. Optical Properties of Ag@ZnO NR System.** The as-prepared samples presented a brownish coloration likely as consequence to the large dispersion of Ag NP sizes. Contrary to this optical behavior, the laser-treated Ag@ZnO NRs samples present a well-defined plasmonic response visually identified by bluish coloration. This different optical behavior is evidenced in Figure 4 showing the extinction spectra recorded at  $0^\circ$  for both the as-prepared and the four irradiated NRs samples. The as-prepared sample depicts a featureless spectrum with a smooth decrease in the extinction from UV to IR, very similar to that reported for pure ZnO films.<sup>41</sup> No relevant changes in the spectral shape occurred before reaching the threshold fluence of  $72 \text{ mJ cm}^{-2}$ , when it develops a broad peak extending from 435 to 550 nm. The development of this band must be associated with the SPR response of the isolated Ag NPs formed within the spherical ZnO particles upon laser treatment. At higher fluences, the extinction coefficient increases and the band broadens toward the IR part of the spectrum.

To further investigate the characteristics of this band, we measured the transmission spectra at  $45^\circ$  with both p- and s-polarized light. The results of this analysis for the as prepared samples and the laser irradiated areas (fluences of  $72 \text{ mJ cm}^{-2}$  and  $130 \text{ mJ cm}^{-2}$ ) are presented in Figure 4b. The spectra taken with s-polarized light are identical to those obtained at  $0^\circ$  (Figure 4a), whereas those recorded with p-polarized light produces an enhancement of the extinction at the UV side of the spectrum (see the clear maximum developing in the range 435–455 nm depending on the fluence), while practically no

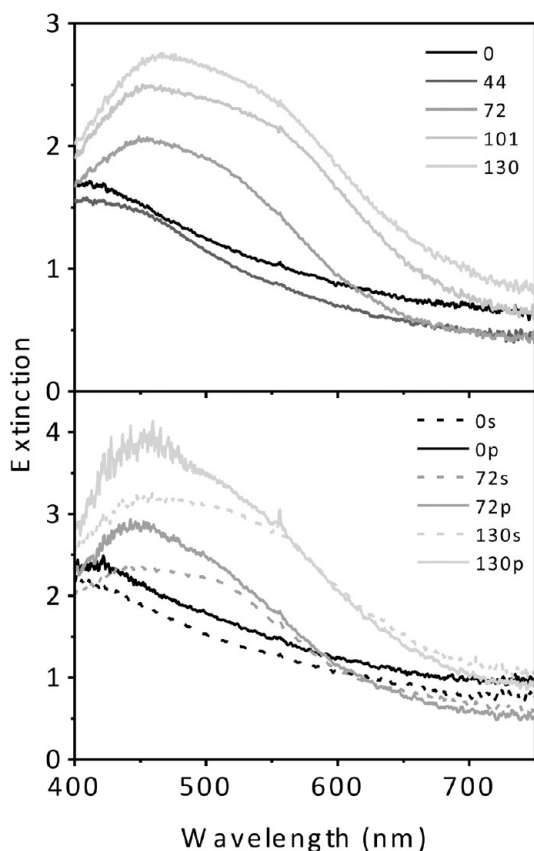


**Figure 4.** (a) Extinction spectra at  $0^\circ$  of laser-treated Ag@ZnO NRs with fluences in  $\text{mJ cm}^{-2}$  as labeled. (b) Extinction spectra of NRs at  $45^\circ$  treated with 72 and  $130 \text{ mJ cm}^{-2}$ , using incident polarized light as labeled. 0 stands for the spectra of as prepared sample.

changes are observed in the IR side (i.e., in the range  $520\text{--}550 \text{ nm}$ ).

**3.3. Ag@ZnO Nanorods as SERS Substrates for Rh6G Detection.** As reported in references,<sup>30,31</sup> in the Ag@ZnO NRs samples, silver NPs with diameters comprised between 3 and 15 nm are distributed in an inner hollow extending along the ZnO NR porous shell structure. The high dispersion of silver NPs and/or aggregates and a likely electronic interaction of the metal phase with the ZnO semiconductor makes this material very attractive for SERS applications.<sup>13,14</sup> An intimate electrical contact between Ag and ZnO was in fact evidenced by the visible photoactivity depicted by these samples.<sup>30</sup>

To check the SERS activity of the Ag@ZnO NRs, Rh6G dye was used as a probe molecule. Figure 5a) illustrates the SERS response after dripping ethanol droplets with different concentrations (from  $1 \times 10^{-11}$  to  $1 \times 10^{-5} \text{ M}$ ) of Rh6G on the as-prepared sample. The spectral features characteristic of Rh6G are clearly identified in the spectra, even for concentrations as low as  $10^{-11} \text{ M}$ . According to literature,<sup>42</sup> the observed peaks can be attributed to the C–C ring in-plane, out-of-plane and C–H in-plane bending vibrations ( $611$ ,  $771$ , and  $1125 \text{ cm}^{-1}$ ), and to symmetric modes of in-plane C–C stretching vibrations ( $1189$ ,  $1360$ ,  $1508$ , and  $1649 \text{ cm}^{-1}$ ). This material presents a high SERS activity with an enhancement factor of about  $1.6 \times 10^6$  (part S6 of the Supporting Information).

The wetting of Ag@ZnO NRs substrates with liquids implies the irreversible formation of a nanocarpets structure.<sup>33</sup> Because of this self-bending and association process, this surface

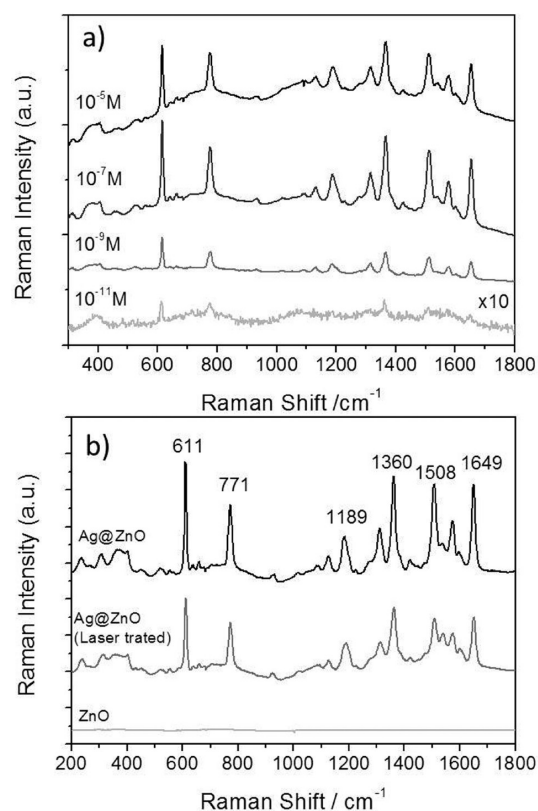


**Figure 5.** (a) SERS spectra of Rh6G collected on as prepared Ag@ZnO NRs for different concentrations (indicated on the upper-left of each spectrum). (b) Comparison between the SERS activity of as prepared NRs, laser-treated NRs, and a ZnO thin film.

transformation produces a decrease in the active surface area which, most likely, is the responsible for the observed small decrease in SERS sensitivity. According to the results in the previous section (c.f. Figure 2), laser-induced morphological changes in the NRs samples offer a way to provide rigidity and stability to the system even after water immersion. Laser irradiation also produces the association of NR tips and affects the Ag NPs distribution (c.f., Figure 2). To check the influence of these morphological differences in the SERS activity, Rh6G SERS spectra were recorded for the as-prepared Ag@ZnO NRs, laser-treated Ag@ZnO NRs and a reference ZnO thin film (Figure 5b). This figure shows that the spectra taken on the laser treated NRs were similar to that on the as-prepared samples. In the two cases all the resonant peaks of Rh6G were recorded, although their intensity was slightly weaker in the former case. Defining the detection efficiency as the ratio between the intensity of the  $771 \text{ cm}^{-1}$  peak of the laser treated with respect to that in the as-prepared NRs, it results that this parameter is close to 90% in the former case. In terms of the enhancement factor, laser-treated NRs present a value of approximately  $1.4 \times 10^6$ . It is also apparent in Figure 5b that the reference ZnO thin film does not present any SERS activity.

An advantageous difference of the laser treated Ag@ZnO NRs with respect to the as-prepared samples was the long lasting detection efficiency achieved in the first case. For analytical purposes, a long lasting stability of the SERS response is an important condition that has been overlooked in previous publications dealing with the SERS activity of Ag-ZnO nanostructures.<sup>13,14</sup> This is a critical issue with zinc oxide-based materials because of their relatively low chemical stability

in water.<sup>43</sup> To evaluate the robustness of our system for SERS, we deposited water droplets with Rh6G and then dried them on the different studied samples. Figure 6 shows the evolution

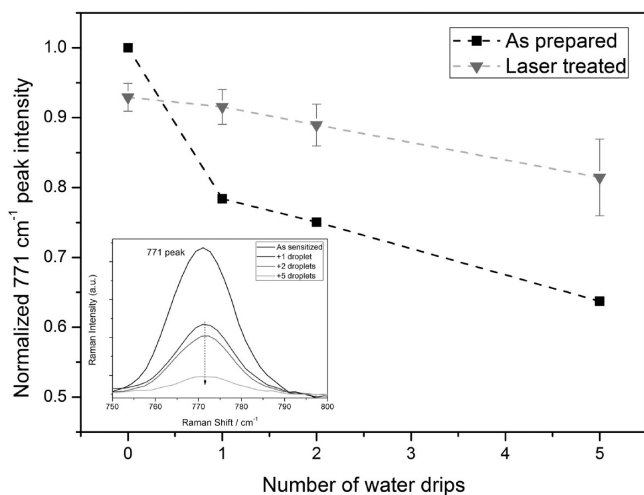


**Figure 6.** Lasting duration test representing the normalized intensity of the 771 cm<sup>-1</sup> Rh6G peak for the as prepared and laser-treated NRs after a series of water drippings. Inset, 771 cm<sup>-1</sup> Rh6G peak evolution after different number of immersions as labeled.

of the normalized intensity of the 771 cm<sup>-1</sup> peak after successive tests. For the as prepared Ag@ZnO NRs, the SERS activity decreased considerably after the first experiment (~80%) and then more slowly to reach 60% of the initial intensity after dripping 5 droplets. By contrast, the laser-treated NRs were more stable and still exhibited 85% of the initial SERS activity after 5 immersions.

## 4. DISCUSSION

**4.1. Laser-Induced Morphological Modification of Ag@ZnO NRs.** The main effect of laser irradiation is the production of bundles of NRs due to the formation of large and almost spherical ZnO particles at the end of the NRs that associate several of them. The morphologies of the particles and bundles are very similar to those reported earlier upon laser irradiation of nondoped ZnO NRs,<sup>37,38</sup> and are related to melting followed by rapid solidification. The melting temperature of ZnO nanorods under conventional slow heating in air has been reported to be ~750 °C, that is significantly lower than that of the bulk material (1700 °C).<sup>44</sup> Annealing during 1 h at this temperature lead to partial melting and coalescence of the nanorods by joining neighboring NRs, whereas the NRs have completely converted into particles upon annealing at ~950 °C. In our case, the porous character of the Ag@ZnO NRs together with the large amount of accumulated defects in their structure might contribute to decrease further the melting temperature. Therefore, we can conclude that laser irradiation for fluences higher than 44 mJ cm<sup>-2</sup> at 193 nm induces melting of the tip of the NRs and the formation of round particles to minimize the free energy. Once the particle size becomes comparable to the NRs separation, neighboring particles coalesce leading to a single bigger particle on top of various NRs, i.e., forming the bundles, similarly to what is observed under conventional annealing at threshold temperature.<sup>44</sup>

Because the melting temperature of bulk silver (960 °C) is close to that of the NRs and that of the initial small Ag NPs in

the porous structure is expected to be at least ~100 °C lower because of their small diameter,<sup>45</sup> we can conclude that the initial Ag NPs have also melted. The low miscibility of Ag and ZnO as well as the high diffusion lengths of atoms within the liquid state compared to those in the solid state promotes phase separation and the aggregation of Ag atoms. This interpretation is supported by the SEM images reported in Figure 2 showing that the Ag NPs are at the surface of the ZnO particles and the absence of aggregation of Ag at the interface with the nonmelted part of the NRs. In agreement with the results reported earlier,<sup>37,38</sup> there is also no evidence for changes in the nonmelted part of the NRs that thus act as crystalline seeds for the solidification of the molten ZnO. It has been reported that the atomic spacing was preserved when passing this interface thus supporting the epitaxial regrowth of the ZnO. XRD and TEM results and the fact that no further changes were observed after successive irradiation treatments are consistent with an epitaxial regrowth occurring also in our case. The fact that a second pulse with same fluence than the first one does not produce further changes evidence that the melting point of the surface material has increased and thus become closer to that of the bulk material and higher than that of the porous NRs. This reasoning is consistent with the ZnO spheres being formed by dense and crystalline ZnO as opposed to the porous structure of the NRs (see Figure S1 and S2 in the Supporting Information) in agreement with the earlier results reported upon laser irradiation of undoped NRs<sup>37,38</sup> and the higher melting temperature of the bulk (dense) material than the porous one.<sup>44</sup>

## 4.2. Optical Properties of Laser-Treated Ag@ZnO NRs.

The brownish color of the as-prepared Ag@ZnO NRs agrees with the wide size distribution of silver NPs found along the inner hollow of these structures. These Ag NPs have diameters in the 3–15 nm range and do not exhibit a well-defined plasmonic response. As suggested earlier,<sup>30</sup> this is likely related to the broad distribution of NP diameters and/or to that an excess of metal infiltrated in the porous ZnO shell prevents the localization of electron oscillations. The ultraviolet nanosecond laser treatment provides a way to modify locally the material surface as well as to produce NPs with plasmonic response. The plasmon band observed in the irradiated zones must be associated with the Ag NPs formed at the ZnO particles at the NR tips as deduced from the SEM analysis of the irradiated samples (c.f. Figure 2).

The spectra recorded at 45° (Figure 4b) with p- and s-polarizations show that the broad plasmonic band response observed at 0° is due to two contributions with relative maxima in the 435–455 nm and 520–555 nm ranges. These two contributions can be accounted for by assuming that the silver NPs formed at the surface of the ZnO particles have an oblate shape with their shorter dimension axis perpendicular to the ZnO spheres. The SPR of similar oblate NPs are known to split into a blue-shifted longitudinal and a red-shifted transversal mode.<sup>4,46</sup> Furthermore, for oblate NPs with an aspect ratio of ~1.5 and embedded in a dielectric media of refractive index ~2.1 (approximately the refractive index of ZnO in the visible region of the spectrum), longitudinal and transversal modes at 445 and 540 nm are expected.<sup>4</sup> These values are very close to the position of the two features observed in the spectra depicted in Figure 4b). In our case, the fact that the blue-mode is enhanced at 45° by using p-polarization, i.e., when the electromagnetic field has a component parallel to the direction of the NRs, suggests that the NPs distribution is not



homogeneous and there is a certain solid angle along the NR axis where they are preferentially located.

**4.3. Long Lasting SERS Devices.** The results reported in Figures 2 and 3 have shown that by laser irradiating the Ag@ZnO NRs, the obtained nanostructure is quite robust and does not experience any nanocarpet formation when immersed in liquids. We attribute this behavior to a high rigidity imparted by the laser formed ZnO nanoparticles to the NRs and to the fact that the long distance separating the associated bundles prevents a capillary driven nanocarpet formation.

The existence of electronic interactions between silver and the ZnO semiconductor in Ag-ZnO composite nanostructures is known to contribute to enhance the SERS sensitivity.<sup>14</sup> In our system, some electron transfer from the Ag NPs to the ZnO NRs should be expected until their Fermi levels attain equilibration. Since the Fermi level of ZnO is lower than that of Ag,<sup>47</sup> ZnO and Ag should get negatively and positively charged, respectively. A certain prevalence of a higher charge-density region at the interface between the Ag-NPs and the ZnO NR should be also expected. This situation must be advantageous for detection via SERS because a localized electromagnetic field excited by a surface plasmon resonance can enhance the Raman scattering of analytes.<sup>14</sup> A scheme of the energy band diagram of the two components illustrating the electron transfer process between Ag nanoparticles and ZnO is displayed in the Figure S7 in the Supporting Information. Results obtained proved that by using this material it is possible to detect concentrations as low as  $1 \times 10^{-11}$  M of Rh6G. We believe that not only the high SERS intrinsic activity of the Ag@ZnO NR structures contributes to enhance the detection sensitivity, but also its high adsorption capacity. The NRs arrays in this sample present a high porosity at two different scales: at the micrometric scale, related with the length of the NRs and the hollow space between them, and at the nanometric scale within the nanocolumns, due to the intrinsic porosity of the ZnO shell.<sup>30</sup> This characteristic nanostructure should lead to a large surface area for molecular adsorption and to an enrichment of analyte molecules.

As-prepared Ag@ZnO NRs undergo a decrease in sensitivity after successive SERS tests (c.f., Figure 6). Different factors should contribute to this decrease in detection efficiency. First, the formation of NR clusters due to the nanocarpet effect tends to minimize the surface in contact with the liquid after the first immersion.<sup>33</sup> Additionally, ZnO tends to dissolve or become hydroxylized in water, hence successive water immersions during SERS tests might result in loss of material and/or in disrupting the electrical contact between ZnO and Ag NPs.<sup>43</sup> Although the latter limitation cannot be easily overcome, our previous results show that laser treated NRs offer an interesting alternative to create a more robust morphology with a longer detection lifespan. Main factor contributing to this improvement is the rigidity of the bundles formed by laser melting and solidification of the upper part of the NRs and a lower degradation of the ZnO melted nanoparticles as compared with that of the porous NRs shell.

## 5. CONCLUSIONS

Laser treatment of Ag@ZnO NRs produce a reshaping of the end of the NRs leading to the formation of bundles terminated by recrystallized ZnO spheres decorated with oblate Ag NPs. These oblate silver NPs exhibit a plasmonic response that is polarization sensitive. The laser-induced modifications render a surface with a higher stability toward SERS detection. The

simplicity of the manufacturing method, not requiring any template or the use of complex techniques, and its compatibility with any kind of substrate material are some of the advantageous features of the procedure.

## ■ ASSOCIATED CONTENT

### Supporting Information

XRD spectra and SEM micrographs of Ag@ZnO NRs laser irradiated with different power fluxes. Picture of a hydrophobic water droplet on top of a Ag@ZnO NRs surface. SEM micrographs of self-bending capillary effect on Ag@ZnO NRs. Calculation of the SERS enhancement factor Energy band diagram of the Ag-ZnO interface. This material is available free of charge via the Internet at <http://pubs.acs.org>.

## ■ AUTHOR INFORMATION

### Corresponding Author

\*E-mail: [maciasmonterom@gmail.com](mailto:maciasmonterom@gmail.com).

### Notes

The authors declare no competing financial interest.

## ■ ACKNOWLEDGMENTS

We thank the Junta de Andalucía (TEP8067, FQM-6900, and P12-FQM-2265) and the Spanish Ministry of Economy and Competitiveness (Projects CONSOLIDER-CSD 2008-00023, MAT2011-28345-C02-02, MAT2013-40852-R, MAT2013-42900-P, and RECUPERA 2020) for financial support. The authors also thank the European Union Seventh Framework Programme under Grant Agreements 312483-ESTEEM2 (Integrated Infrastructure Initiative-I3) and REGPOT-CT-2011-285895-AI-NANOFUNC, and the European Research Council under the European Union's Seventh Framework Programme (FP/2007-2013)/ERC grant agreement 291522-3DIMAGE. R.J.P. acknowledges the grant JCI-2012\_13034 from the Juan de la Cierva program.

## ■ ABBREVIATIONS

CS, cross section  
NP, nanoparticle  
NR, nanorod  
PECVD, plasma enhanced chemical vapor deposition  
PL, photoluminescence  
Rh6G, rhodamine 6G  
SEM, scanning electron microscopy  
SERS, surface enhanced Raman scattering  
SPR, surface plasmon resonance

## ■ REFERENCES

- (1) Chang, W. S.; Slaughter, L. S.; Khanal, B. P.; Manna, P.; Zubarev, E. R.; Link, S. One-Dimensional Coupling of Gold Nanoparticle Plasmons in Self-Assembled Ring Superstructures. *NanoLett.* **2009**, *9*, 1152–1157.
- (2) Kreibitz, U. M. V.; Vollmer, M. *Optical Properties of Metal Clusters*; Springer: Berlin, 1995.
- (3) Murray, W. A.; Barnes, W. L. Plasmonic Materials. *Adv. Mater.* **2007**, *19*, 3771–3782.
- (4) Noguez, C. Surface Plasmons on Metal Nanoparticles: The Influence of Shape and Physical Environment. *J. Phys. Chem. C* **2007**, *111*, 3806–3819.
- (5) El Ahrach, H. I.; Bachelot, R.; Vial, A.; Lerondel, G.; Plain, J.; Royer, P.; Soppera, O. Spectral Degeneracy Breaking of the Plasmon Resonance of Single Metal Nanoparticles by Nanoscale Near-Field Photopolymerization. *Phys. Rev. Lett.* **2007**, *98*, 107402.

- (6) Gonzalez-Garcia, L.; Parra-Barranco, J.; Sanchez-Valencia, J. R.; Ferrer, J.; Garcia-Gutierrez, M. C.; Barranco, A.; Gonzalez-Elipe, A. R. Tuning Dichroic Plasmon Resonance Modes of Gold Nanoparticles in Optical Thin Films. *Adv. Funct. Mater.* **2013**, *23*, 1655–1663.
- (7) Fort, E.; Ricolleau, C.; Sau-Pueyo, J. Dichroic Thin Films of Silver Nanoparticle Chain Arrays on Faceted Alumina Templates. *NanoLett.* **2003**, *3*, 65–67.
- (8) Filippin, A. N.; Borrás, A.; Rico, V. J.; Fruto, F.; González-Elipe, A. R. Laser Induced Enhancement of Dichroism in Supported Silver Nanoparticles Deposited by Evaporation at Glancing Angles. *Nanotechnology* **2013**, *24*, 045301.
- (9) Bakker, R. M.; Yuan, H. K.; Liu, Z. T.; Drachev, V. P.; Kildishev, A. V.; Shalaev, V. M.; Pedersen, R. H.; Gresillon, S.; Boltasseva, A. Enhanced Localized Fluorescence in Plasmonic Nanoantenna. *Appl. Phys. Lett.* **2008**, *92*, 043101.
- (10) Baruah, S.; Dutta, J. Nanotechnology Applications in Pollution Sensing and Degradation in Agriculture: a Review. *Environ. Chem. Lett.* **2009**, *7*, 191–204.
- (11) Kneipp, K.; Kneipp, H.; Kneipp, J. Surface-Enhanced Raman Scattering in Local Optical Fields of Silver and Gold Nanoparticles. *Acc. Chem. Res.* **2006**, *39*, 443–450.
- (12) Mulvihill, M.; Tao, A.; Benjauthrit, K.; Arnold, J.; Yang, P. Surface-Enhanced Raman Spectroscopy for Trace Arsenic Detection in Contaminated Water. *Angew. Chem.* **2008**, *120*, 6556–6560.
- (13) Yin, J.; Zang, Y.; Yue, C.; Wu, Z.; Wu, S.; Li, J.; Wu, Z. Ag Nanoparticle/ZnO Hollow Nanosphere Arrays: Large Scale Synthesis and Surface Plasmon Resonance Effect Induced Raman Scattering Enhancement. *J. Mater. Chem.* **2012**, *22*, 7902–7909.
- (14) Tang, H.; Meng, G.; Huang, Q.; Zhang, Z.; Huang, Z.; Zhu, C. Arrays of Cone-Shaped ZnO Nanorods Decorated with Ag Nanoparticles as 3D Surface-Enhanced Raman Scattering Substrates for Rapid Detection of Trace Polychlorinated Biphenyls. *Adv. Funct. Mater.* **2012**, *22*, 218–224.
- (15) Chen, T.; Xing, G. Z.; Zhang, Z.; Chen, H. Y.; Wu, T. Tailoring the Photoluminescence of ZnO Nanowires Using Au Nanoparticles. *Nanotechnology* **2008**, *19*, 435711.
- (16) Zang, Y.; He, X.; Li, J.; Yin, J.; Li, K.; Yue, C.; Wu, Z.; Wu, S.; Kang, J. Band Edge Emission Enhancement by Quadrupole Surface Plasmon–Exciton Coupling Using Direct-Contact Ag/ZnO Nanospheres. *Nanoscale* **2013**, *5*, 574–580.
- (17) Wang, H.; Ruan, W.; Zhang, J.; Yang, B.; Xu, W.; Zhao, B.; Lombardi, J. R. Direct Observation of Surface-Enhanced Raman Scattering in ZnO Nanocrystals. *J. Raman Spectrosc.* **2009**, *40*, 1072–1077.
- (18) Li, X. H.; Chen, G. Y.; Yang, L. B.; Jin, Z.; Liu, J. H. Multifunctional Au-Coated TiO<sub>2</sub> Nanotube Arrays as Recyclable SERS Substrates for Multifold Organic Pollutants Detection. *Adv. Funct. Mater.* **2010**, *20*, 2815–2824.
- (19) Zhang, M. L.; Fan, X.; Zhou, H. W.; Shao, M. W.; Zapien, J. A.; Wong, N. B.; Lee, S. T. A High-Efficiency Surface-Enhanced Raman Scattering Substrate Based on Silicon Nanowires Array Decorated with Silver Nanoparticles. *J. Phys. Chem. C* **2010**, *114*, 1969–1975.
- (20) Wang, X.; Kong, X.; Yu, Y.; Zhang, H. Synthesis and Characterization of Water-Soluble and Bifunctional ZnO–Au Nanocomposites. *J. Phys. Chem. C* **2007**, *111*, 3836–3841.
- (21) Morton, S. M.; Jensen, L. Understanding the Molecule–Surface Chemical Coupling in SERS. *J. Am. Chem. Soc.* **2009**, *131*, 4090–4098.
- (22) Zhang, B.; Wang, H.; Lu, L.; Ai, K.; Zhang, G.; Cheng, X. Large-Area Silver-Coated Silicon Nanowire Arrays for Molecular Sensing Using Surface-Enhanced Raman Spectroscopy. *Adv. Funct. Mater.* **2008**, *18*, 2348–2355.
- (23) Cheng, C.; Yan, B.; Wong, S. M.; Li, X.; Zhou, W.; Yu, T.; Shen, Z.; Yu, H.; Fan, H. J. Fabrication and SERS Performance of Silver-Nanoparticle-Decorated Si/ZnO Nanotrees in Ordered Arrays. *ACS Appl. Mater. Interfaces* **2010**, *2*, 1824–1828.
- (24) Chen, J. Y.; Saeki, F.; Wiley, B. J.; Cang, H.; Cobb, M. J.; Li, Z. Y.; Au, L.; Zhang, H.; Kimmey, M. B.; Li, X. D.; Xia, Y. N. Gold Nanocages: Bioconjugation and Their Potential Use as Optical Imaging Contrast Agents. *NanoLett.* **2005**, *5*, 473–477.
- (25) Qin, Y.; Wang, X. D.; Wang, Z. L. Microfibre–Nanowire Hybrid Structure for Energy Scavenging. *Nature* **2008**, *451*, 809–813.
- (26) Suh, W. H.; Jang, A. R.; Suh, Y. H.; Suslick, K. S. Porous, Hollow, and Ball-in-Ball Metal Oxide Microspheres: Preparation, Endocytosis, and Cytotoxicity. *Adv. Mater.* **2006**, *18*, 1832–37.
- (27) Li, X. L.; Lou, T. J.; Sun, X. M.; Li, Y. D. Highly Sensitive WO<sub>3</sub> Hollow-Sphere Gas Sensors. *Inorg. Chem.* **2004**, *43*, 5442–5449.
- (28) Mathiowitz, E.; Jacob, J. S.; Jong, Y. S.; Carino, G. P.; Chickering, D. E.; Chaturvedi, P.; Santos, C. A.; Vijayaraghavan, K.; Montgomery, S.; Bassett, M.; Morrell, C. Biologically Erodeable Microspheres as Potential Oral Drug Delivery Systems. *Nature* **1997**, *386*, 410–414.
- (29) Yamada, T.; Iwasaki, Y.; Tada, H.; Iwabuki, H.; Chuah, M. K.; VandenDriessche, T.; Fukuda, H.; Kondo, A.; Ueda, M.; Seno, M.; Tanizawa, K.; Kuroda, S. Nanoparticles for the Delivery of Genes and Drugs to Human Hepatocytes. *Nat. Biotechnol.* **2003**, *21*, 885–890.
- (30) Macias-Montero, M.; Borrás, A.; Saghi, Z.; Romero-Gomez, P.; Sanchez-Valencia, J. R.; Gonzalez, J. C.; Barranco, A.; Midgley, P.; Cotrino, J.; Gonzalez-Elipe, A. R. Superhydrophobic Supported Ag-NPs@ZnO-Nanorods with Photoactivity in the Visible Range. *J. Mater. Chem.* **2012**, *22*, 1341–1346.
- (31) Macias-Montero, M.; Borrás, A.; Saghi, Z.; Espinos, J. P.; Barranco, A.; Cotrino, J.; Gonzalez-Elipe, A. R. Vertical and Tilted Ag-NPs@ZnO Nanorods by Plasma-Enhanced Chemical Vapour Deposition. *Nanotechnology* **2012**, *23*, 255303.
- (32) Kamalasanan, M. N.; Chandra, S. Sol-Gel Synthesis of ZnO Thin Films. *Thin Solid Films* **1996**, *288*, 112–115.
- (33) Macias-Montero, M.; Borrás, A.; Alvarez, R.; Gonzalez-Elipe, A. R. Following the wetting of one-dimensional photoactive surfaces. *Langmuir* **2012**, *28*, 15047–15055.
- (34) Nadarajah, A.; Könenkamp, R. Laser Annealing of Photoluminescent ZnO Nanorods Grown at Low Temperature. *Nanotechnology* **2011**, *22*, 025205.
- (35) Lin, T. N.; Huang, C. P.; Shu, G. W.; Shen, J. L.; Hsiao, C. S.; Chen, S. Y. Influence of Pulsed Laser Annealing on the Optical Properties of ZnO Nanorods. *Phys. Status Solidi A* **2012**, *209*, 1461–1466.
- (36) Shimogaki, T.; Okazaki, K.; Nakamura, D.; Higashihata, M.; Asano, T.; Okada, T. Effect of laser annealing on photoluminescence properties of Phosphorus implanted ZnO nanorods. *Opt. Express* **2012**, *20*, 15247–15252.
- (37) Maeng, J.; Heo, S.; Jo, G.; Choe, M.; Kim, S.; Hwang, H.; Lee, T. The effect of Excimer Laser Annealing on ZnO Nanowires and Their Field Effect Transistors. *Nanotechnology* **2009**, *20*, 095203.
- (38) Wang, X.; Ding, Y.; Yuan, D.; Hong, J. I.; Liu, Y.; Wong, C. P.; Hu, C.; Wang, Z. L. Reshaping the Tips of ZnO Nanowires by Pulsed Laser Irradiation. *Nano Res.* **2012**, *5*, 412–420.
- (39) Sanchez-Valencia, J. R.; Toudert, J.; Borrás, A.; Barranco, A.; Lahoz, R.; de la Fuente, G. F.; Frutos, F.; Gonzalez-Elipe, A. R. Selective Dichroic Patterning by Nanosecond Laser Treatment of Ag Nanostripes. *Adv. Mater.* **2011**, *23*, 848–853.
- (40) Sanchez-Valencia, J. R.; Toudert, J.; Borrás, A.; Lopez-Santos, C.; Barranco, A.; Ortega Feliu, I.; Gonzalez-Elipe, A. R. Tunable In-Plane Optical Anisotropy of Ag Nanoparticles Deposited by DC Sputtering onto SiO<sub>2</sub> Nanocolumnar Films. *Plasmonics* **2010**, *5*, 241–250.
- (41) Aydogu, S. O.; Coban, M. B. The Optical and Structural Properties of ZnO Thin Films Deposited by the Spray Pyrolysis Technique. *Chin. J. Phys.* **2012**, *50*, 89.
- (42) Tang, H.; Meng, G.; Huang, Q.; Zhang, Z.; Huang, Z.; Zhu, C. Arrays of Cone-Shaped ZnO Nanorods Decorated with Ag Nanoparticles as 3D Surface-Enhanced Raman Scattering Substrates for Rapid Detection of Trace Polychlorinated Biphenyls. *Adv. Funct. Mater.* **2012**, *22*, 218–224.
- (43) Zhou, J.; Xu, N.; Wang, Z. L. Dissolving Behavior and Stability of ZnO Wires in Biofluids: A Study on Biodegradability and



Biocompatibility of ZnO Nanostructures. *Adv. Mater.* **2006**, *18*, 2432–2435.

(44) Su, X.; Zhang, Z.; Zhu, M. Melting and Optical Properties of ZnO Nanorods. *Appl. Phys. Lett.* **2006**, *88*, 061913.

(45) Luo, W.; Hu, W.; Xiao, S. Size Effect on the Thermodynamic Properties of Silver Nanoparticles. *J. Phys. Chem. C* **2008**, *112*, 2359–2369.

(46) Margueritat, J.; Gonzalo, J.; Afonso, C. N.; Bachelier, G.; Mlayah, A.; Laarakker, A. S.; Murray, D. B.; Saviot, L. From Silver Nanolentils to Nanocolumns: Surface Plasmon-Polaritons and Confined Acoustic Vibrations. *Appl. Phys. A: Mater. Sci. Process.* **2007**, *89*, 369–372.

(47) Sun, Z.; Wang, C.; Yang, J.; Zhao, B.; Lombardi, J. R. Nanoparticle Metal–Semiconductor Charge Transfer in ZnO/PATP/Ag Assemblies by Surface-Enhanced Raman Spectroscopy. *J. Phys. Chem. C* **2008**, *112*, 6093–6098.